Am J Physiol Lung Cell Mol Physiol 294: L87–L97, 2008.
First published November 16, 2007; doi:10.1152/ajplung.00186.2007.

Alteration of deposition pattern and pulmonary response as a result of improved dispersion of aspirated single-walled carbon nanotubes in a mouse model

R. R. Mercer,[1,2] J. Scabilloni,[1] L. Wang,[1] E. Kisin,[1] A. R. Murray,[1] D. Schwegler-Berry,[1] A. A. Shvedova,[1,2] and V. Castranova[1,2]

[1]*Pathology and Physiology Research Branch, Health Effect Laboratory Division, National Institute for Occupational Safety and Health, Morgantown; and* [2]*Department of Physiology and Pharmacology, West Virginia University, Morgantown, West Virginia*

Submitted 10 May 2007; accepted in final form 11 November 2007

Mercer RR, Scabilloni J, Wang L, Kisin E, Murray AR, Schwegler-Berry D, Shvedova AA, Castranova V. Alteration of deposition pattern and pulmonary response as a result of improved dispersion of aspirated single walled carbon nanotubes in a mouse model. *Am J Physiol Lung Cell Mol Physiol* 294: L87–L97, 2008. First published November 16, 2007; doi:10.1152/ajplung.00186.2007.—Nanoparticles have a fundamental dimension of <100 nm. However, on suspension in media, agglomerates of nanoparticles are the more common structure. This is particularly evident in prior intratracheal instillation or aspiration studies of single-walled carbon nanotubes (SWCNT), in which granulomatous lesions encased by epithelioid macrophages were produced by large agglomerates. In this study, we tested the hypothesis of whether exposure to more dispersed SWCNT structures would alter pulmonary distribution and response. A dispersed preparation of single-walled carbon nanotubes (DSWCNT) with a mean diameter of 0.69 μm was given by pharyngeal aspiration to C57BL/6 mice. Electron microscopy demonstrated a highly dispersed, interstitial distribution of DSWCNT deposits by 1 day postexposure. Deposits were generally <1 μm. Macrophage phagocytosis of DSWCNT was rarely observed at any time point. Lung responses were studied by lavage and morphometry at 1 h, 1 day, 7 day, and 1 mo after a single DSWCNT exposure of 10 μg/mouse. Lung sections and lavage cells demonstrated an early, transient neutrophilic and inflammatory phase that rapidly resolved and was similar to that observed with large agglomerates. No granulomatous lesions or epithelioid macrophages were detected. Morphometric measurement of Sirius red staining was used to assess the connective tissue response. The average thickness of connective tissue in alveolar regions was 0.10 ± 0.02, 0.09 ± 0.02, 0.10 ± 0.01, 0.48 ± 0.04, and 0.88 ± 0.19 μm for PBS and 1-h, 1-day, 7-day, and 1-mo postexposure groups, respectively. The results demonstrate that dispersed SWCNT are rapidly incorporated into the alveolar interstitium and that they produce an increase in collagen deposition.

toxicology; nanoparticles; particulates; emerging technologies; lung injury

SINGLE-WALLED CARBON NANOTUBES (SWCNT) are a new form of carbon arranged in a two-dimensional graphene sheet that is rolled into a tube of nanometer diameter. These nanometer-sized tubes align with adjacent tubes via van der Waals forces to form nanoropes of 20–50 nm diameter (6). Agglomerates form from these, generating a wide range of particle-sized structures in the micrometer range. As a consequence of the structural form, SWCNT have an extraordinary strength-to-weight ratio and are highly resistant to environmental weathering. SWCNT are used in applications requiring individual nanotubes or nanoropes, as well as in applications where weaves or aggregates of SWCNT are used for structural support, protective coatings, or high-power current transmission. Because of the exceedingly low density of the SWCNT, inhalation of SWCNT clumps manyfold larger than those normally considered as an inhalation risk must be evaluated. For instance, the mass-equivalent aerodynamic diameter of a 20-μm-diameter SWCNT agglomerate may be <0.3 μm. Mild agitation, such as might be induced by a worker manipulating the material, produces mainly micrometer-sized clumps of particles (14). However, high energy can produce aerosols of submicrometer-sized structures (P. Baron, unpublished observations).

There are relatively few toxicity studies of SWCNT. Lam et al. (10) were the first to report the granulomatous lesions in the mouse 7 and 90 days after intratracheal instillation of SWCNT. This research demonstrated that, on an equal-weight basis, SWCNT were more toxic than carbon black or quartz. Warheit et al. (26) conducted higher dose intratracheal instillation studies in the rat, which demonstrated granulomatous lesions but also reported that the granulomas were not dose dependent and that exposure to large agglomerates obstructed conducting airways, causing asphyxiation in a large percentage of exposed animals. They concluded that the high doses and large agglomerates resulted in an artifactual response that was not relevant to likely human exposure. In a subsequent pharyngeal aspiration study, Shvedova et al. (19) demonstrated that purified SWCNT (low-iron contamination) produce a significant granulomatous response associated with deposition sites of agglomerates. This study also demonstrated a progressive fibrotic response in the alveolar parenchyma that did not appear to rely on inflammatory cell mechanisms in the later stages of development and that was not associated with the sites exhibiting granulomatous response. These results suggest that a dispersed or submicrometer form of SWCNT, which was not detectable by light microscopic means, could be responsible for the alveolar wall connective tissue response. More recently, Mangum et al. (13) conducted similar experiments that also demonstrated the fibrotic response and found that

Address for reprint requests and other correspondence: R. R. Mercer, Health Effects Laboratory, NIOSH, Morgantown, WV 26505 (e-mail: rmercer@cdc.gov).

The costs of publication of this article were defrayed in part by the payment of page charges. The article must therefore be hereby marked "*advertisement*" in accordance with 18 U.S.C. Section 1734 solely to indicate this fact.

SWCNT were able to form focal adhesions or bridges between alveolar macrophages, which may serve as a biomarker for nanotube exposure.

As evident from the studies described above, the pulmonary response to SWCNT is subject to debate, varying from a non-dose-dependent reaction to a dose-dependent progressive interstitial fibrotic response. The hypothesis to be tested in the present study is whether the deposition pattern and pulmonary reaction to SWCNT structure depend on the degree of dispersion in the exposure suspension.

In the present study, we report results using a combination of a number of different approaches to determine whether a population of dispersed SWCNT is present in suspensions used for pharyngeal aspiration in the study by Shvedova et al. (19) study and to test the possible health effects of a more dispersed suspension of purified SWCNT. To provide a direct test of the effect of improved SWCNT dispersion on toxicity, dispersed SWCNT (DSWCNT) were prepared and used for comparisons to the responses obtained with the less dispersed SWCNT preparation. Two different labeling processes were used to identify the distribution of both the less dispersed SWCNT and the more dispersed SWCNT preparations: labeling with 10-nm colloidal gold and labeling with fluorescent quantum dots. With the use of these labels, it was possible to identify the distribution of the more dispersed SWCNT form in the lungs, to determine whether the less dispersed SWCNT preparation also contained finer structures, and to determine where those finer structures were distributed.

MATERIALS AND METHODS

Animals. Specific pathogen-free adult male C57BL/6 mice (24 wk) were supplied by Jackson Laboratory (Bar Harbor, ME). Animals were individually housed in Association for Assessment and Accreditation of Laboratory Animal Care-accredited National Institute for Occupational Safety and Health animal facilities in microisolator cages for at least 1 wk before use. Autoclaved Beta Chip bedding (Northeastern Products, Warrensburg, NY) was changed weekly. Animals were supplied with water and Harlan Teklad 7913, NIH-31 modified mouse/rat diet, irradiated (Harlan Teklad, Madison, WI), and housed under controlled light, temperature, and humidity conditions. Animals were monitored on a daily basis for morbidity, illness, and adverse effects, with none noted. All methods involving animals were conducted under protocols approved by our Institutional Animal Care and Use Committee.

Carbon nanotube source and dose. SWCNT purified from a high-pressure carbon monoxide production process (HiPCO) with <2 wt% of contaminants (CNI, Houston, TX) were used for preparation of DSWCNT. A dose of 10 μg/mouse was used for both SWCNT and DSWCNT exposures. This dose is the lowest of those used in our prior studies of responses to SWCNT (19).

Experimental groups and time points. Animals were studied at 1 h after pharyngeal aspiration to determine the initial deposition pattern and at 1 day, 7 day, and 1 mo postexposure to determine the acute inflammatory response, chronic fibrotic response, and fate of the aspirated carbon nanotube (CNT). A PBS-treated group was used as the control. Six mice, given DSWCNT or SWCNT, were studied at each time point for measurement of connective tissue and alveolar responses by morphometry. Bronchoalveolar lavage (BAL) analysis was done at each time point with six animals per group given DSWCNT. Additional groups were given gold-labeled DSWCNT ($n = 4$) or quantum dot-labeled DSWCNT ($n = 4$). These groups were studied at 1 h and at 1, 3, and 7 days after aspiration. To control for the possibility of unbound label, additional groups of mice were given aspirations of 0.1 μg of colloidal gold or 0.25 μg of quantum dots. The doses were chosen based on the amount of bound gold or quantum dots in the 10 μg/mouse gold-labeled DSWCNT and 10 μg/mouse quantum dot-labeled DSWCNT studies, respectively. These animals were studied 1 day after aspiration. A morphometric analysis of the fate of these unbound labels was conducted to identify how the lung processed unbound label.

Pharyngeal aspiration. This alternative to inhalation has been described in detail elsewhere (17). Briefly, after anesthetization, the animal was placed on a board in a near vertical position and the animal's tongue was extended with padded forceps. A suspension of the material to be aspirated (50 μl/mouse) at the desired concentration or PBS vehicle was placed on the back of the tongue. A slight pull of the tongue results in a reflex gasp and aspiration of the droplet. The tongue was held, and the animal was monitored for a few breaths after aspiration. To eliminate the possibility of incidental food aspiration, food was removed 4 h before the procedure; water was removed 1 h before the procedure.

BAL cell counting. The degree of inflammatory response induced by the pharyngeal-aspirated particulates was estimated by the total cells, macrophages, neutrophils, and lymphocytes recruited into the mouse lungs and recovered by BAL. BAL of mice was conducted as previously described by our laboratory (28). Mice were weighed and killed with an intraperitoneal injection of pentobarbital sodium (>100 mg/kg). The trachea was cannulated with a blunted 22-gauge needle, and BAL was performed using cold sterile Ca^{2+}- and Mg^{2+}-free PBS at a volume of 1 ml/lavage for six lavages with a total of ~5 ml of BAL fluid per mouse collected and pooled. Centrifuge slide preparations were then prepared from the lavage fluid. Cell counts were performed to identify alveolar macrophages and polymorphonucleocytes (PMN) based on their characteristic cell shape in centrifuge slide preparations stained with the Hema-3 kit (Fisher Scientific, Pittsburgh, PA), and differential counts of BAL cells were conducted. Three hundred cells per slide were counted.

Vascular perfusion fixation of the lungs. Preservation of the lungs was done by vascular perfusion of fixative. This method of fixation was chosen to eliminate the possible disturbance of deposited materials or cells in the air spaces. Methods for vascular perfusion fixation were as previously reported (16) with the basic goal being to preserve the lungs at a state comparable to that present at end expiratory volume. For this procedure, the animal was anesthetized (75 mg/kg Nembutal) by intraperitoneal injection. Once a deep level of anesthesia was obtained, a tracheal cannula was inserted and a laparotomy was performed. The animal was then euthanized by exsanguination. The pulmonary artery was cannulated via the ventricle, and an outflow cannula was inserted into the left atrium. In quick succession, the tracheal cannula was connected to a 5 cmH_2O pressure source to inflate the lungs with air, and clearing solution was perfused via the pulmonary artery. After blood was cleared from the lungs, the perfusate was switched to fixative consisting of 2% glutaraldehyde, 1% formaldehyde, and 1% tannic acid with sucrose as an osmotic agent. Tannic acid was included to produce an electron-dense staining of connective tissue fibers and to assist in preservation of lipid structures in the lungs. Clearing solution consisted of a physiological salt solution containing heparin (100 U/ml) and adjusted to 350 mosM with sucrose.

Fixed lung volume was measured by water displacement. Longitudinal sections were cut from the lungs. The lungs were embedded in paraffin and sectioned at a thickness of 5 μm for light microscopy. For electron microscopy, tissue blocks were en bloc stained with uranyl acetate and embedded in epoxy resin. Ultra-thin sections (60 nm) were cut, stained with uranyl acetate and lead citrate, and examined by a transmission electron microscope (JEOL JEM-1220).

Cryo fixation. Animals were anesthetized with pentobarbital sodium (75 mg/kg) by intraperitoneal injection and euthanized by exsanguination. The trachea was cannulated. An incision was made just below the sternum, and both hemidiaphragms were punctured to

deflate the lungs. The lungs were then slowly inflated with 0.8 ml of a cryomix over a 1-min period. After inflation, the lungs were excised from the chest, placed in a cryomold, and covered with chilled OCT (Tissue-Tek; Sakura Finetek, Torrance, CA). The lungs-cryomold were then frozen in dry ice-cooled isopentane (−40°C to −50°C) and stored at −80°C until sectioned. A cryomicrotome was used to cut sections 4 μm thick. The lung tissue sections were mounted on slides and vapor fixed with vapors from a heated 2% paraformaldehyde solution. The cryomix consisted of 70% by volume OCT and 30% by volume of a 30% by weight sucrose-PBS solution.

Sirius red staining for collagen detection. Collagen in the lungs was detected with Sirius red staining (8), which has been demonstrated to be a quantitative morphometric method for collagen determination in the lungs (1, 12). Paraffin sections were deparaffinized and rehydrated with xylene-alcohol series to distilled water. The slides were then stained with 0.1% Picrosirius solution (100 mg of Sirius red F3BA in 100 ml of saturated aqueous picric acid, pH 2) for 1–2 h, washed for 1 min in 0.01 N HCl, counterstained with Mayer's hematoxylin for 2 min, dehydrated, and mounted with a coverslip.

Morphometric analysis. Quantitative morphometric methods were used to measure the average thickness of Sirius red-positive connective tissues in the alveolar regions. Volume and surface densities were measured by standard morphometric analyses (15, 25). This consisted of basic point and intercept counting. Volume density was determined from counting the number of points over the Sirius red-positive connective tissues in the alveolar regions and points over Sirius red-positive connective tissues and cells in the granulomatous regions. Surface density of the alveolar wall and granulomatous regions were determined from intercepts between a line overlay and the alveolar wall. These point and intercept counts were made with a 121-point, 11-line overlay graticule (12.5 mm^2 with 100 divisions) at ×100 magnification taken at six locations equally spaced across each section (one section per animal). This process was repeated twice for each animal. To limit the measurements to alveolar parenchyma, areas containing airways or blood vessels >25 mm in diameter were excluded from the analysis. Average thickness of the Sirius red-positive connective tissues of the alveolar wall was computed from two times the ratio of volume density of point to the surface density of the alveolar wall.

Preparation of dispersed SWCNT. Two hundred milligrams of purified SWCNT (low iron) were initially suspended in 60 ml of distilled water, passed through a 200-mesh stainless steel screen to grossly separate the material, and sonicated for 10 min. The solution was then expanded to 200 ml with acetone and placed in an ultrasonic bath maintained at room temperature for 24 h. When dispersed in acetone, there was an approximately 150-fold increase in the volume of the SWCNT sample compared with that in distilled water. This was due to the dissociation of nanotubes as the nonionic solvent, acetone, reduced the van der Waals forces binding the CNTs (27). The dispersed SWCNT were then filtered from the solution using two stages of a 20-μm nylon mesh screen, which had a 4-μm hole diameter (CMN-0029-C, Small Parts, Miami Lakes, FL). The acetone solution containing the DSWCNT was then passed through a 0.2-μm polytetrafluoroethylene (PTFE) filter, which had been weighed before use. After collection on the filter, the DSWCNT were washed several times with distilled water to remove residual acetone. The filter was dried overnight in vacuum and weighed to determine the quantity of DSWCNT (typically 5–10 mg). Before use, the filter containing the DSWCNT was placed in PBS and DSWCNT were released into solution by brief sonication. Acetone and PBS were prefiltered with a 0.2-μm PTFE filter before use. To assess the size distribution of the DSWCNT and SWCNT samples, a sample of each was taken, diluted to decrease loading density, and filtered onto a 25-mm diameter, 0.1-μm pore polycarbonate filter (VCTP02500 isopore membrane; Millipore, Billerica, MA). The polycarbonate filter was then washed with distilled water and dried. Micrographs of the CNT particles on the filter were then taken with a scanning electron microscope. The area equivalent diameter of the DSWCNT and SWCNT was then determined. The distribution of average area equivalent diameter of the DSWCNT was approximately normally distributed with a mean of 0.69 μm and a variance of 0.49 with a maximum area equivalent diameter of 3.7 μm. The area equivalent diameter of the SWCNT was approximately normally distributed with a mean of 15.2 μm and a variance of 3.2 μm. The improvement in dispersion was demonstrated by microscopic evaluation of the suspensions before aspiration, as shown in Fig. 1.

Colloidal gold labeling of CNT. For preparation of gold-labeled CNT, a 0.1-mg sample of SWCNT or DSWCNT was dispersed in distilled water. The sample was then filtered onto a 0.1-μm PTFE filter. (The PTFE filter was wetted with a trace amount of methanol before use.) The CNT-PTFE filter was then incubated in a sulfuric acid-nitric acid (3:1 vol/vol) solution for 1 h to produce sufficient carboxylate groups in the carbon atom matrix of the SWCNT to attach a gold particle every 100–200 nm of nanorope length. This procedure is a mild version of the high heat pressure, concentrated acid bath used to remove iron, graphite, and soot in the refinement of purified CNT

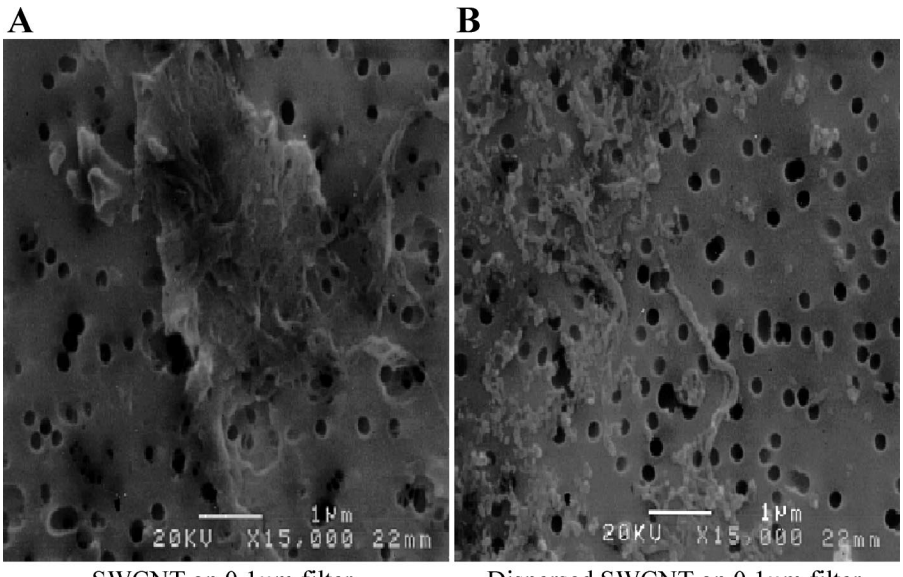

Fig. 1. Scanning electron microscope images of suspensions of single-walled carbon nanotubes (SWCNT; *A*) and dispersed preparation of single-walled carbon nanotubes (DSWCNT; *B*) before aspiration (collected on polycarbonate filters). Circular holes are the 0.1-μm pores of the filter.

(21). Without the acid treatment, gold particle labeling was reduced by 75%, thus demonstrating that the additional acid treatment produced relatively minor additional functional groups on the CNT. After the acid incubation, the CNT-PTFE filter was rinsed in multiple exchanges of distilled water until the pH was ~7.0. The CNT-PTFE filter was incubated in a 10-nm colloidal gold solution, pH 9.0, (polygold GC; Polysciences, Warrington, PA), which was monodispersed before use by sonication and filtration on a submicrometer filter. After 15 min, filtered BSA was added to a final concentration of 5% BSA to stabilize the gold particles and to assist in removal of unbound gold particles. Tris·HCl-saline with 1% BSA at pH 8.2 was then passed through the CNT-PTFE filter five or six times to remove any unbound colloidal gold. The filter was rinsed with Tris·HCl-saline and then rinsed with distilled water and stored dried on the filter until it was used. Before aspiration, the filter was rinsed with PBS and CNT were released from the PTFE filter by brief sonication.

Silver enhancement of gold-labeled CNT in sections. For light microscope visualization of the gold-labeled CNT, paraffin sections were deparaffinized and dehydrated. The sections were then washed with multiple changes of deionized water. Sections were developed with a silver enhancement kit designed for gold labels (BB International, Cardiff, UK). The reaction was terminated after 15 min of development by washing in deionized water, and then the sections were lightly stained with Sirius red to improve detection of the silver deposits. Sections from PBS-treated controls and lungs given unlabeled SWCNT were used to control for background silver development in sections.

Fluorescent quantum dot labeling of CNT. SWCNT or DSWCNT were labeled with fluorescent quantum dots (30 nm in diameter). For this purpose, CNT were conjugated with an amine functionalized Fort orange fluorochrome, EviDots binding kit (T2-MP; Evident Technologies, Troy, NY). Two hundred micrograms of acid-treated CNT (SWCNT or DSWCNT) were filtered onto a 0.2-μm PTFE filter. The material was rinsed with distilled water to pH 7 and then labeled with quantum dots according to the EviTag conjugation protocol, which is a modification of a procedure first described by Grabarek and Gergely (5). Labeled CNT were then released into PBS solution by brief sonication.

Laser scanning confocal microscopy. For study of quantum dot-labeled CNT, lungs from animals treated by pharyngeal aspiration of Fort orange-labeled quantum dots were cyropreserved and sectioned. Images from the sections were recorded with a Zeiss LSM 510 confocal microscope using a ×60 objective with a pixel size of 290 nm. The tissue was imaged by differential interference contrast, and the Fort orange-labeled quantum dots were imaged with a 543-nm HeNe laser for excitation, with a 560-nm long-pass filter to capture the red-orange emission of the quantum dots.

To study the collagen distribution by confocal imaging, 5-μm-thick paraffin sections were deparaffinized and transferred to ethanol. The sections were then fluorescently labeled by incubation for 24 h with a 0.1 mg/ml concentration of Lucifer yellow-CH according to manufacturer's protocol (Molecular Probes, Eugene, OR). Sections were then rinsed in ethanol for 5 min and coverslipped. Images were recorded with a ×60 objective with excitation of 488 nm and emission spectra >510 nm used to image the fluorescently labeled collagen.

Statistical analyses. Data were analyzed by ANOVA (STATGRAF). Bartlett's test was used to test for homogeneity of variances between groups. Statistical differences were determined by one-way ANOVA, with significance set at $P \leq 0.05$. When significant F-values were obtained, individual means were compared with control using two-sided Dunnett's test (3), and $P < 0.05$ was considered to be significant. Data are given as means ± SE.

RESULTS

Micrographs of lungs exposed to DSWCNT or SWCNT demonstrate a similar pattern of inflammatory response, i.e., a rapid but transient PMN recruitment. Figure 2 shows PMN within alveolar spaces at 1 day postexposure but no PMN at 7 days postexposure. Further analyses of histological sections of the lungs (Fig. 2) indicated that no visible deposits of DSWCNT were observed in association with either neutrophils or alveolar macrophages. No significant airway involvement in the inflammatory process was observed. The number of lavage macrophages was elevated between *day 1* and *7*. However,

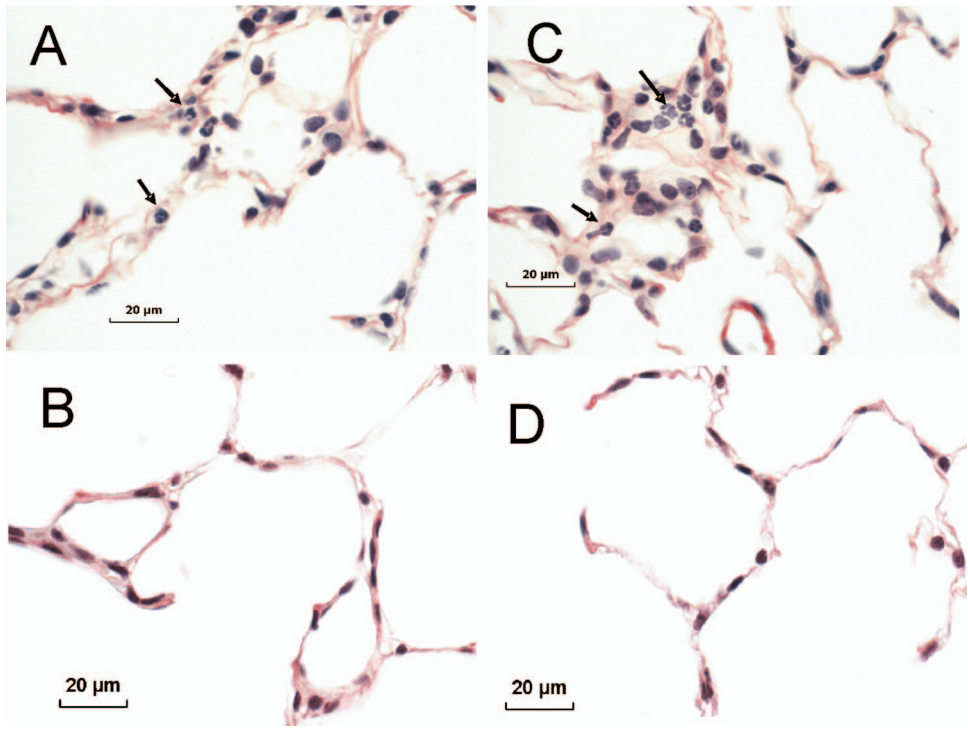

Fig. 2. Micrographs showing transient polymorphonuclear (PMN) recruitment after SWCNT or DSWCNT exposure. Both SWCNT (*A*) and DSWCNT (*C*) produced a transient PMN recruitment into the alveolar walls of the lungs 1 day postexposure (arrows). Seven days after exposure, no significant PMN recruitment remained for either SWCNT (*B*) or DSWCNT (*D*). Sections were stained with Sirius red.

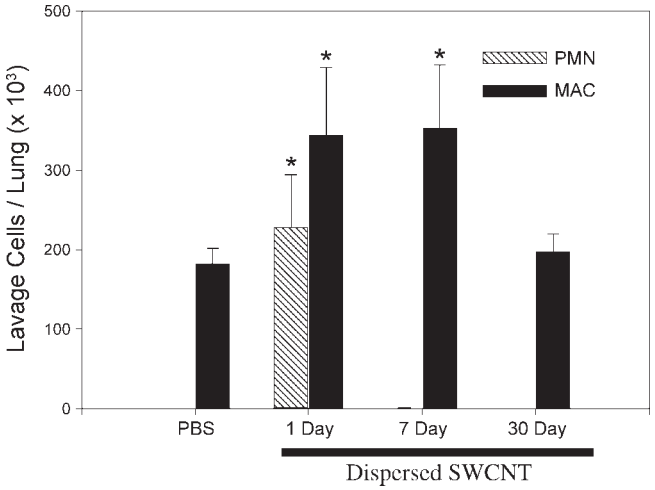

Fig. 3. Cell differential of bronchoalveolar lavage (BAL) samples from mice after pharyngeal aspiration of 10 μg/mouse of DSWCNT (1 day, 7 days, and 30 days) or PBS. PMNs in BAL demonstrated a transient response during the first few days after aspiration, which resolved by *day 7*. Lavage macrophages (MAC) were elevated above control levels (PBS) but returned to control values at 30 days. Values are means ± SE; $n = 6$ mice. *$P < 0.05$ vs. PBS-treated control mice.

macrophages observed by transmission electron microscope were generally normal in appearance and did not reveal morphological evidence of activation, such as flattening of the cell or increased cell ruffling and filopodia.

Figure 3 presents a quantitation of BAL cell counts for lungs after pharyngeal aspiration of 10 μg/lung DSWCNT, demonstrating a transient neutrophil influx that resolved within 7 days. This PMN response was similar in time course and magnitude to that previously reported for aspiration of less dispersed SWCNT (19). Lavage analysis of alveolar macrophages indicated that an increase in alveolar macrophages of ~60% over the PBS controls occurs in response to DSWCNT at 1–7 days postexposure and returns to control at 30 days. This magnitude of alveolar macrophage response was similar to that previously observed for less dispersed SWCNT (19). Overall, the inflammatory sequence as indicated by BAL analysis and examination of lung sections was consistent with a mild, transient parenchymal inflammation that developed and was resolved within the first week of exposure.

Although CNT are unreactive to light microscopic stains, large agglomerates, 2–20 μm in diameter, can readily be identified in lung sections from animals given the less dispersed SWCNT because the mass of SWCNT in the section is sufficient to block light transmission. The lung response to these large agglomerates of less dispersed SWCNT results in infiltration and encasement by epithelioid macrophages to form a connective tissue-rich granulomatous inflammation that is typical of the lungs response to an insoluble particle (Fig. 4*A*). The epithelioid macrophages in the transmission electron micrograph are larger than typical alveolar macrophages and have a paucity of lysosomes and phagolysosomes and an organelle-poor cytoplasm with long, thin digitations that are characteristic of epithelioid macrophages (11, 22, 24). As shown in Fig. 4, the long, thin digitations of epithelioid macrophages separate or "wall-off" the insoluble SWCNT agglomerates from the lungs. Significant collagen and elastin fibers were also observed within the lesions associated with deposition of agglomerates of SWCNT, as previously reported (19). Figure 4*B* shows the distribution of a granuloma in the proximal alveolar region of a mouse 7 days after exposure to less dispersed SWCNT. In contrast, such granulomatous lesions are absent in lungs exposed to DSWCNT (Fig. 4*C*).

We made attempts to determine the distribution of DSWCNT in sections from mice that were given the unlabeled material. Because of its much smaller size, the DSWCNT deposition could not be easily observed. Only rarely was it possible to

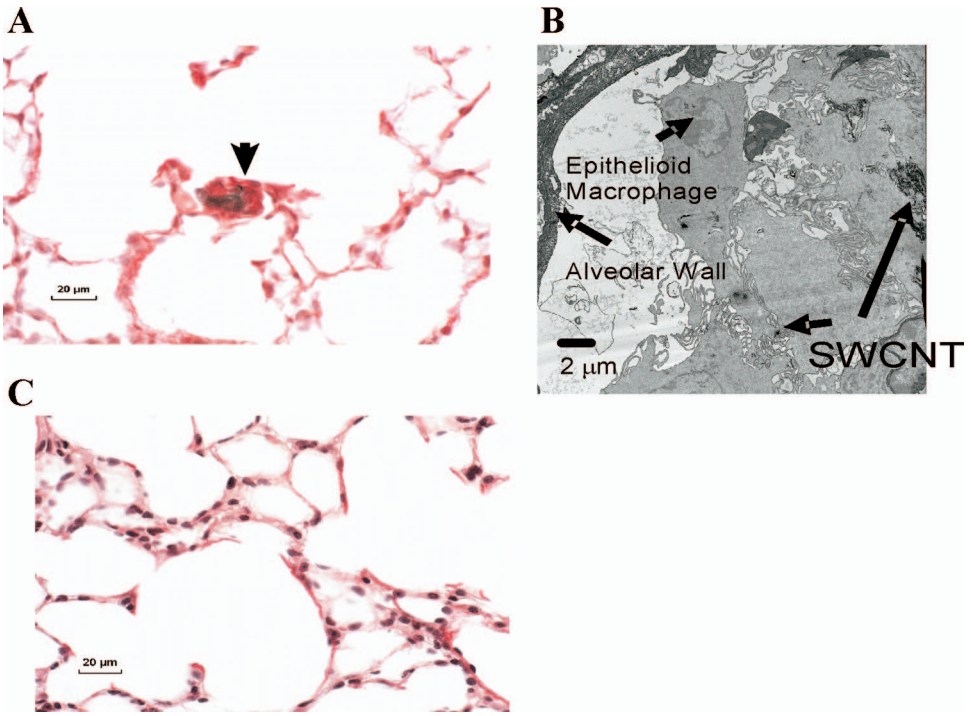

Fig. 4. Gross lung responses to SWCNT and DSWCNT. *A*: large masses of SWCNT infiltrated with collagen are readily observed in sections 7 days postexposure to SWCNT. *B*: transmission electron microscope image showing a cross section through a portion of a granuloma 30 days after exposure to SWCNT. As illustrated by this micrograph, SWCNT granulomas are extensively infiltrated with connective tissue and encased by epithelioid macrophages, which have significant inclusions with the aspirated SWCNT. Arrows indicate SWCNT deposits in the granuloma. *C*: in lung sections from animals given DSWCNT, carbon nanotubes cannot be identified without the use of special labeling, as shown in subsequent figures.

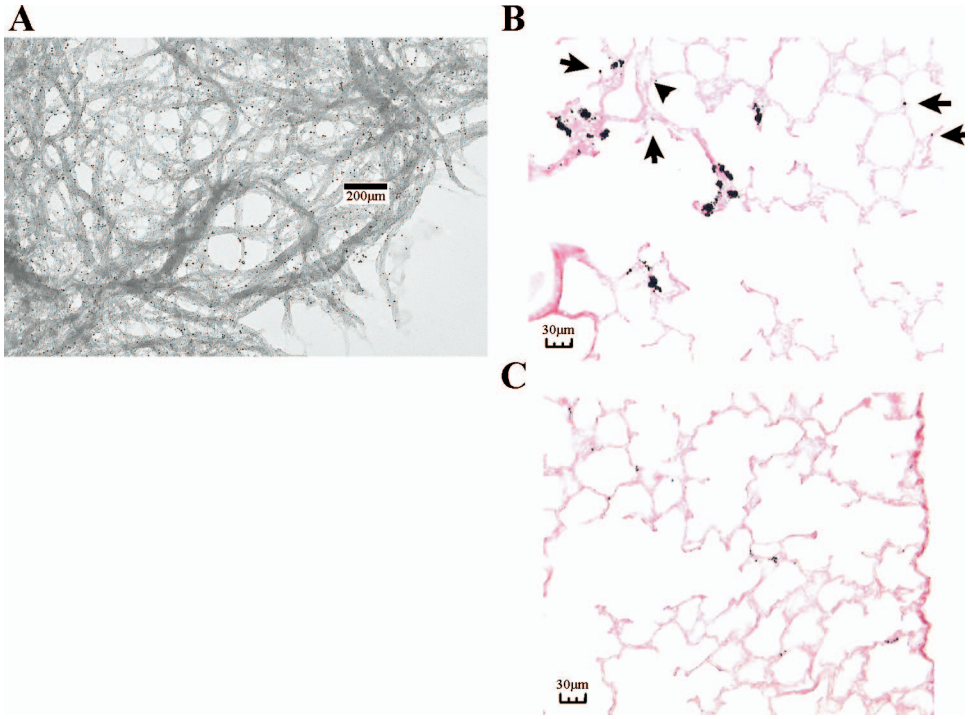

Fig. 5. Gold-labeled carbon nanotubes. *A*: electron micrograph of a gold-labeled SWCNT sample before aspiration showing the 10-nm gold particles (black dots) along the nanotubes. *B* and *C*: regional distributions of SWCNT (*B*) and DSWCNT (*C*) at 1 day postexposure. The large black deposits of silver enhancement of the SWCNT-exposed lung (*B*) are concentrated near the proximal alveolar region. These are the areas where granulomatous lesions form about the large agglomerates of SWCNT. Finer structures of less dispersed SWCNT, corresponding to the small black deposits (arrows), can be seen distributed widely throughout the lungs. These smaller structures were not visible before silver enhancement. In *C*, silver-enhanced sections from lungs of mice given gold-labeled DSWCNT showed a much finer and diffuse pattern of deposition.

identify deposition of DSWCNT in ordinary light microscopic sections. Such deposits were typically 1–3 μm in diameter. Fortunately, the gross distribution of all size classes of CNT was easily discernable in the silver-enhanced sections from animals given gold-labeled SWCNT or DSWCNT. Figure 5*A* is an electron micrograph showing the typical labeling density for a gold-labeled less dispersed SWCNT before aspiration. Gold-labeled DSWCNT produced a similar labeling density (data not shown). Figure 5, *B* and *C*, shows representative low-magnification light micrographs of silver-enhanced detection of gold-labeled nanotubes (SWCNT and DSWCNT, respectively). Figure 5*B* demonstrates the distribution of gold-labeled, less dispersed SWCNT showing large black structures that were concentrated near the proximal alveolar region. This is the main area where granulomatous lesions form after administration of less dispersed SWCNT preparations. Small black dots corresponding to submicrometer deposits of this SWCNT preparation can also be identified throughout the alveolar region. We estimate that these submicrometer structures constitute ~20% of the total of less dispersed SWCNT material in the lungs based on the morphometric point counting of these sections. Silver-enhanced sections from lungs of mice given the gold-labeled DSWCNT showed a much finer and diffuse pattern of deposition, as illustrated in Fig. 5*C*. DSWCNT were identified throughout the interstitial spaces and in the vicinity of the pleura. Occasional deposits were also identified within alveolar macrophages, but these were <5% of the total by point counting of silver-enhanced sections. Deposition of DSWCNT in conducting airways was minimal. Figure 6 demonstrates the typical nanorope fragment interactions with lung cells, which were observed within alveolar macrophages and the alveolar interstitium within 1 day of aspiration of gold-labeled DSWCNT. Figure 6*A* shows two inclusions within an alveolar macrophage containing gold-labeled nanoropes (arrows indicate the gold label). Such engulfment of DSWCNT by alveolar macrophages was relatively rare. Figure 6*B* shows the much more typical finding of gold-labeled DSWCNT in the alveolar interstitial space. Background silver deposits per unit area of tissue section were determined in sections from PBS controls and estimated to account for <2% of the silver deposits in treated sections. In practice, it was possible to distinguish between background silver deposits and those developed

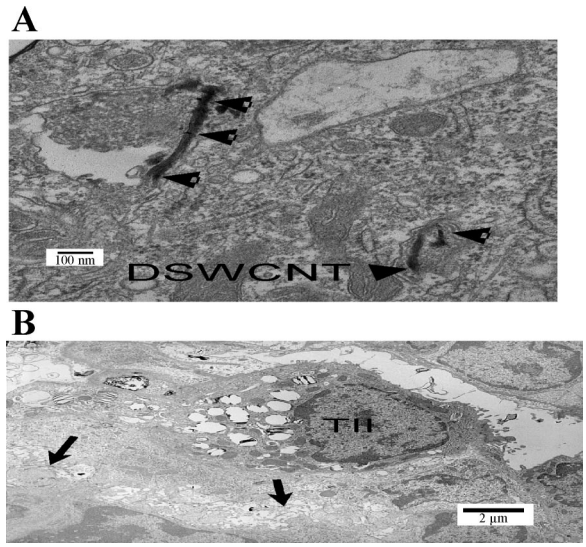

Fig. 6. Electron micrographs of gold-labeled DSWCNT. *A* and *B*: lung cell interactions with DSWCNT that were identified by gold-labeled DSWCNT. Occasional alveolar macrophages were found that contained DSWCNT within apparent cytoplasmic inclusions (arrowheads in *A*). The majority of the DSWCNT identified were 1- to 2-μm packets found in the alveolar interstitium, as illustrated by the 2 small nanotubes indicated by arrows beneath an alveolar type II (TII) epithelial cell in *B*.

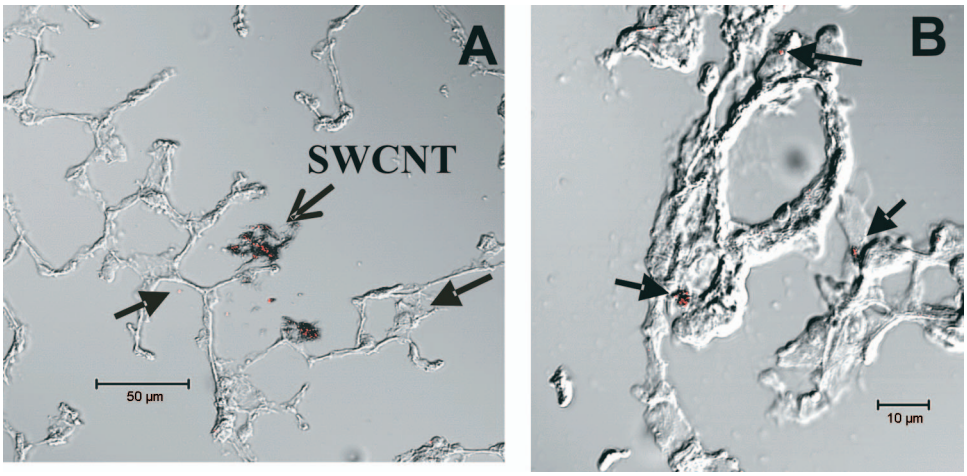

Fig. 7. Quantum dot labeling of SWCNT and DSWCNT in the lungs. Frozen lung sections were imaged by differential interference contrast to view tissue and fluorescence (red) and to view the quantum dot-labeled SWCNT (*A*) and DSWCNT (*B*). Large agglomerates of labeled, less dispersed SWCNT with red-orange fluorescence label are readily apparent in *A* (open arrow); also shown are much smaller and previously unidentified nanotube structures in the air spaces and interstitium (closed arrows). In *B*, arrows indicate Fort orange-labeled DSWCNT, which have migrated into the alveolar interstitium.

from the presence of a gold label because the gold-labeled CNT generated a grapelike cluster of rounded silver deposits due to the multiple gold nucleation sites for silver binding, whereas background silver deposits were single and irregular to sharp-edged silver deposits.

Confocal imaging of frozen sections was used to identify fluorescently labeled less dispersed SWCNT and DSWCNT. To obtain a focal, high-intensity fluorescent signal, the nanotubes were conjugated to a quantum dot Fort orange fluorochrome (Fig. 7). One hour and one day after aspiration, these deposits were observed in the alveolar air spaces. The large agglomerates of less dispersed SWCNT (open arrow) in the air spaces are readily apparent without the red fluorescent label due to their direct effect on the phase of light as detected by interference contrast. As illustrated in Fig. 7*A*, there were additional smaller nanotube structures identified due to the presence of red fluorescent label in both the air spaces (closed arrow) and in the interstitium (closed arrow). By 7 days, only the large agglomerates remained in the air spaces. The pattern of deposition of DSWCNT, with the majority of the nanotubes incorporated within the alveolar interstitial spaces within the first day, is shown in Fig. 7*B*.

Study of lung sections from animals given free colloidal gold or quantum dots was conducted. Paraffin sections from animals given unbound gold particles were processed and silver enhanced. In contrast to the gold bound to DSWCNT, practically all of the free gold were found to be phagocytized by alveolar macrophages (Fig. 8*A*). Greater than 97% of the free particles were found within alveolar macrophages. Of the remaining 3%, approximately half were judged to be due to background noise in the silver enhancement step. Similarly, we examined frozen sections of the animals given unbound quantum dots and conducted counts of the location of the particles with a confocal microscope using the fluorescence mode to find each particle and the differential interference contrast mode to identify lung tissue. In contrast to the quantum dots bound to DSWCNT, all but a few percent of the free particles were phagocytized by alveolar macrophages (Fig. 8*B*).

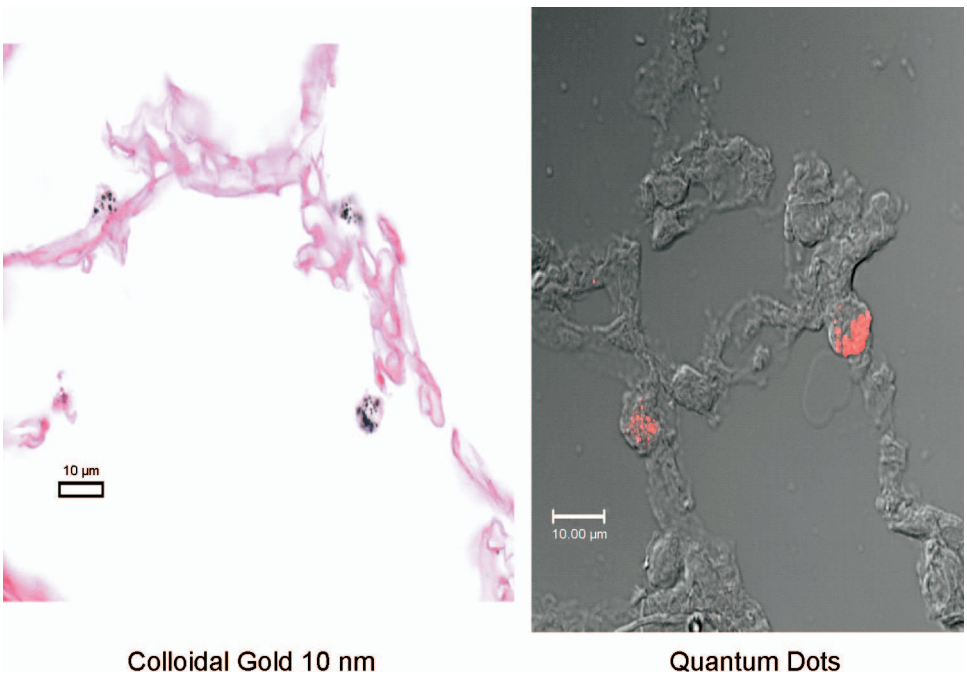

Fig. 8. Light micrographs of lung sections from animals given unbound colloidal gold or quantum dots. *A*: silver-enhanced section from an animal 1 h after aspiration of colloidal gold. *B*: confocal image of a lung section from an animal 1 h after aspiration of quantum dots. Both unbound colloidal gold and quantum dots are rapidly and essentially completely phagocytized by alveolar macrophages.

Table 1. *Body weight and lung morphometry after DSWCNT exposure*

Group	Body Weight, g	Lung Volume, ml	Alveolar Surface Area, cm^2	Alveolar Gas Volume, ml	Alveolar Tissue Volume, ml
PBS DSWCNT	33.0±1.5	0.89±.03	567±60	0.51±0.03	0.19±0.01
1 h	33.5±1.5	0.99±0.14	586±83	0.57±0.09	0.19±0.03
1 day	32.7±1.2	0.98±0.04	512±44	0.53±0.03	0.17±0.02
7 day	34.1±0.7	1.06±0.08	521±42	0.57±0.04	0.18±0.02
30 day	33.6±0.7	0.92±0.04	564±26	0.50±0.03	0.22±0.02

Values are means ± SE. Mice were given 10 μg of dispersed single-wall carbon nanotubes (DSWCNT) at indicated times before death or were given PBS (control).

Basic results for the PBS and DSWCNT groups prepared for morphometric analysis by vascular perfusion fixation are given in Table 1. In this experiment, age of the mice at exposure was staggered so that there were no significant differences between groups for body weight, fixed lung volume, alveolar surface area, or alveolar region gas volume at the time of death.

The average thicknesses of collagen in the alveolar wall for the PBS and DSWCNT groups are given in Fig. 9. As shown in Fig. 9, DSWCNT dramatically increased the collagen content of the alveolar wall in a time-dependent manner. At 1 h and 1 day after aspiration, collagen content was comparable to that of the PBS control. A significant increase was observed at *day 7* and progressed, without further exposure, by *day 30*. This time course is consistent with our prior study (19) of lung collagen changes for less dispersed SWCNT, in which significant collagen production was noted 7 days postexposure with continued increases at longer time points. However, DSWCNT were more potent in inducing interstitial collagen accumulation than an equal mass aspiration of the less dispersed SWCNT preparation as shown in Fig. 10.

Figure 10 shows representative confocal fluorescence microscope images of sections stained with Lucifer yellow to detect the collagen distribution. In a normal lung, the edges of the alveolar septa that contain the alveolar entrance rings are the most prominent site of collagen (15). The collagen distribution of mice 1 day after aspiration of dispersed SWCNT or DSWCNT was not different from the PBS-treated groups. As illustrated in Fig. 10, areas of significant collagen accumulation in the alveolar wall were found 7 and 30 days after aspiration of dispersed SWCNT and DSWCNT (arrows); however, the distribution of such collagen accumulation differed. Most of the abnormal collagen deposition in the SWCNT-treated lungs was associated with agglomerates of SWCNT in the lungs. In contrast, collagen accumulation in DSWCNT-treated lungs was widely distributed within the alveolar walls throughout the lungs. Morphological evaluation indicated that DSWCNT caused more extensive interstitial collagen accumulation than the less dispersed SWCNT.

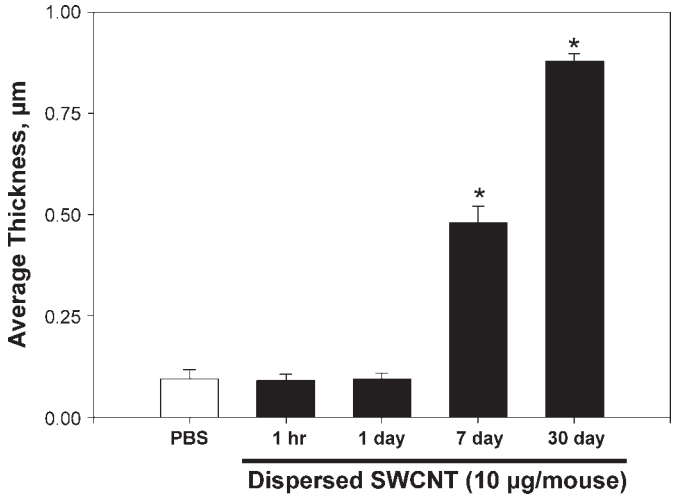

Fig. 9. Morphometric changes in alveolar wall collagen fiber content. Results from determination of the average thicknesses of alveolar wall connective tissue fibers at various times after aspiration of DSWCNT are given. At 7 days, there was significant accumulation of connective tissue fibers in the alveolar wall, which continued to increase through 30 days after aspiration. Values are means ± SE; $n = 6$ mice. *$P < 0.05$ vs. PBS-treated control mice.

DISCUSSION

In any study in which binding of labels is used to identify the distribution of nanomaterials, attention has to be focused on the possibility that the label will become unbound from the nanoparticles and/or that the label when bound will alter the lung response to the nanoparticles. As indicated in RESULTS, a number of steps were taken to detect whether the label became detached from the CNT. It was demonstrated that both gold and quantum dot labeling agents, when used alone, were avidly phagocytized and concentrated within alveolar macrophages. If either label were to become unbound from the CNT in the lungs, the unbound label would be concentrated within alveolar macrophages and thus easily detected. No unbound label was detected within alveolar macrophages for either label in our studies with less dispersed SWCNT or DSWCNT.

A more difficult issue to address is the possibility that the label alters the response of SWCNT in lungs. As demonstrated in the results, both gold and quantum dots are rapidly phagocytized by macrophages. We had concerns that attachment of the label to the CNT would induce avid phagocytosis by macrophages. For this reason, we intentionally conducted the labeling reactions under conditions that favored the lowest labeling density, which would still provide the capacity for detection. In comparing the lungs given the labeled CNT with unlabeled CNT, we were unable to identify any differences in response. Gold labeling of less dispersed SWCNT produced granulomas similar to those shown for unlabeled less dispersed SWCNT. Gold-labeled DSWCNT were rapidly incorporated within the alveolar interstitium and did not produce granulomatous lesions, as was the case for unlabeled DSWCNT. Similar results were found for quantum dot labeling of both less dispersed SWCNT and DSWCNT. Thus there was no

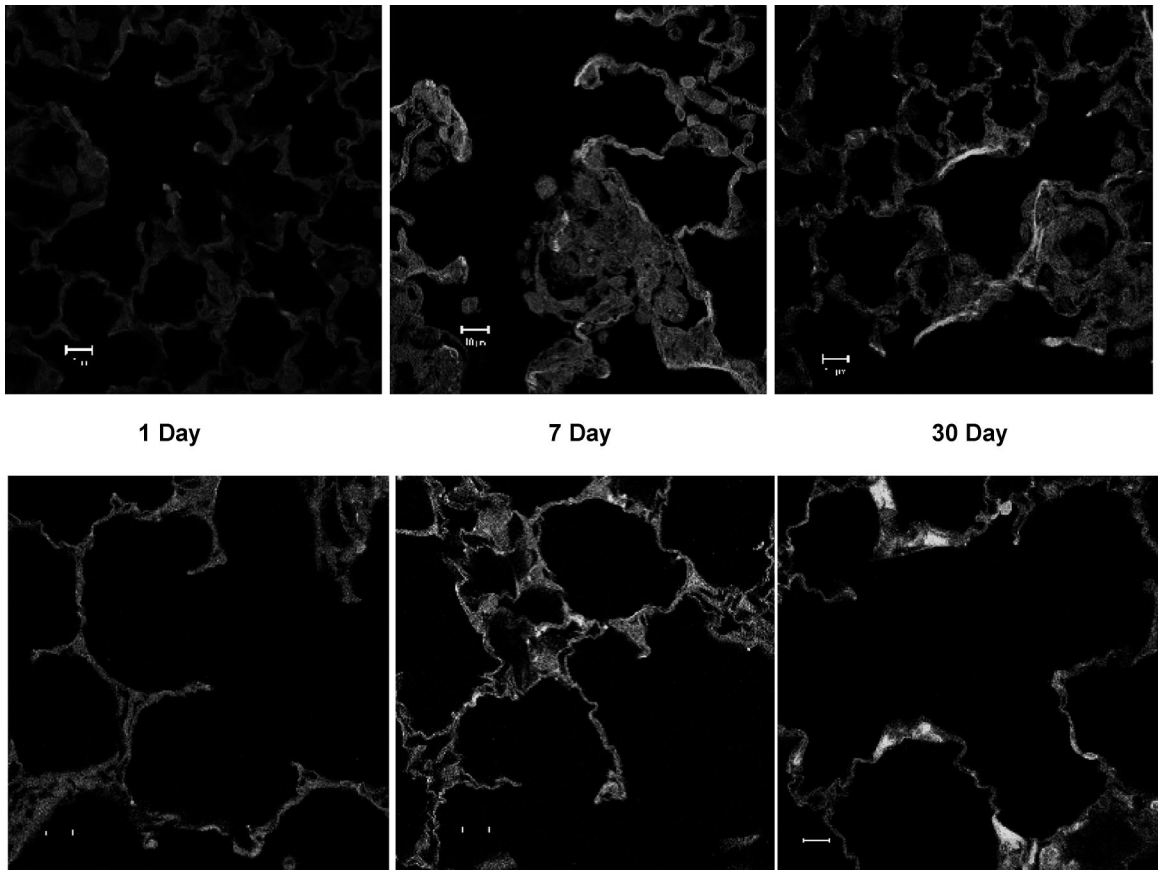

Fig. 10. Confocal fluorescence microscopy of Lucifer yellow-stained lung sections for detection of collagen in SWCNT- and DSWCNT-exposed lungs. Shown are representative images from animals 1 day, 7 days, and 1 mo after aspiration of SWCNT (*top*) and DSWCNT (*bottom*). There was no significant difference in the collagen distribution 1 day after aspiration of SWCNT or DSWCNT. Areas of abnormal collagen deposition were observed at *day 7* and *day 30* after aspiration of SWCNT and DSWCNT. The abnormal collagen deposition in the SWCNT-treated lungs was typically associated with agglomerates of SWCNT in the lungs. Abnormal collagen in DSWCNT-treated lungs was widely distributed within the alveolar walls throughout the lungs.

evidence for differences in how the lungs processed or responded to labeled or unlabeled CNT for either of the two distinctly different labels.

In earlier studies, Lam et al. (10) noted that areas not directly associated with the deposition of SWCNT agglomerates appear "thicker" than normal but did not identify the cause. We demonstrated that DSWCNT produce significant increases in interstitial collagen and further showed that a significant fraction of the administered less dispersed SWCNT is deposited in the lungs as smaller nanorope structures. Based on our labeling studies, we also demonstrated that the small nanorope structures penetrate into the alveolar interstitium. For the less dispersed SWCNT preparation, ~80% of the material is in the large agglomerate form, which, at least initially, remains in the air spaces and ultimately develops into granulomas; 20% of the SWCNT material is small enough to enter the alveolar walls and stimulate interstitial collagen accumulation.

Typically, SWCNT have been administered in PBS and are prone to rapid agglomeration. In PBS, SWCNT agglomerate within 1 min and can even be observed to agglomerate while being vortexed. Ultrasonication immediately before use can significantly reduce this problem and can result in deposits within the lungs with a diameter of ~15 μm (9, 19). Once deposited in the lungs, the action of surfactant and protein may reduce van der Waals interactions between nanotubes and disperse these agglomerates. The dispersive action of alveolar-lining fluid on nanoparticles has been demonstrated in vitro (18). Evidence exists that improved dispersion of ultrafine carbon black in alveolar-lining fluid increases the inflammatory potential of the dust in vivo (20). In the present study, improved dispersion of CNT altered the distribution from agglomerates in the proximal alveoli to dispersed structures in the alveolar walls and pulmonary responses from granulomatous to an interstitial fibrotic reaction. Our study using both gold and quantum dot labeling of less dispersed SWCNT demonstrates that a significant fraction of the aspirated SWCNT material may exist as a submicrometer fraction that can rapidly migrate into alveolar interstitial spaces. The morphological evaluation of the distribution of labeled CNT indicates that relatively little of this material is a target for macrophage engulfment and phagocytosis. Results from in vitro studies by Kagan et al. (9) found little evidence for macrophage phagocytosis, whereas the study of Cherukuri et al. (2) using cells suspended in chemical surfactant demonstrated active ingestment. These differences may reflect differences in the state of the SWCNT samples used. For instance, purified SWCNT is low in iron, whereas raw SWCNT is rich in iron particles that may stimulate phagocytosis. Alternatively, the use of chemical surfactants in the incubation may enhance membrane permeabilities.

Studies to date have been limited to the responses during the first 30–60 days of exposure to SWCNT. Freshly produced CNT have a low chemical functionalization (21). Our observed low-labeling densities obtained by both gold and quantum dot labels and the low propensity for phagocytosis (9) are consistent with the idea that freshly manufactured SWCNT are not highly functionalized. This suggests that lung responses might begin to diminish at some time after the initial deposition and dispersion. However, the lungs are known to have a high oxidant-generating potential compared with other organs and also continually produce and reprocess large quantities of surfactants that may act as dispersive agents on the SWCNT. Over longer time frames, SWCNT encased in granulomas may be altered sufficiently to be released in a form that is either more readily recognized by macrophages or incorporated into the alveolar interstitial spaces. A delayed release of dispersed and more highly functionalized SWCNT would likely have adverse consequences.

The exposure level of DSWCNT was 10 μg/mouse lung in the present investigation. Maynard et al. (14) monitored respirable dust levels during laboratory handling of SWCNT and reported peaks of 53 $\mu g/m^3$. With an assumption of a minute ventilation of 20,000 ml/min during light work (4) and 21% alveolar deposition of 0.69 μm of DSWCNT (7), 106.8 μg of DSWCNT would be predicted to deposit on the alveolar epithelial surface of a worker per day. Normalizing to the equivalent alveolar epithelial surface area in the human (102 m^2/lung) and mouse (0.05 m^2/lung) from published morphometric analysis (23), one can calculate that workers would receive a unit alveolar lung burden equivalent to pharyngeal aspiration of 10 μg of DSWCNT in the mouse in ~200 workdays. Therefore, one can conclude that the exposure level of DSWCNT used in the present study is relevant to potential occupational exposures.

In conclusion, there are at least three principal pathways for dissemination of SWCNT in the lungs. In general, ~80% of the less dispersed material deposits in the lungs as large agglomerates that result in rapidly forming granulomatous lesions in the alveolar region immediately proximal to the small airways. The remaining portion of less dispersed nanotubes appears to be aspirated as smaller structures and/or is dispersed by the lung milieu into a finer form, which is widely distributed throughout the air spaces of the lung parenchyma and is rapidly incorporated into the alveolar interstitial wall, inducing increased collagen production that progresses in the absence of persistent inflammation. A relatively small fraction of the purified SWCNT was found to be engulfed or otherwise processed by alveolar macrophages. Improved dispersal of SWCNT results in aspiration of smaller structures that are more prone to enter the alveolar walls. The pulmonary response to DSWCNT is a more potent interstitial fibrotic reaction in the absence of granuloma formation.

ACKNOWLEDGMENTS

We thank Dr. Lyndell Millecchia, Dean Newcomer, and Sherri Friend for contributions to the pathological analysis work in this paper.

The findings and conclusions in this report are those of the authors and do not necessarily represent the views of the National Institute for Occupational Safety and Health.

REFERENCES

1. **Antonini JM, Hemenway D, Davis G.** Quantitative image analysis of lung connective tissue in murine silicosis. *Exp Lung Res* 26: 71–88, 2000.
2. **Cherukuri P, Bachilo SM, Litovsky SH, Weisman RB.** Near-infrared fluorescence microscopy of single-walled carbon nanotubes in phagocytic cells. *J Am Chem Soc* 126: 15638–15639, 2004.
3. **Dunnett CW.** New tables for multiple comparisons with a control. *Biometrics* 20: 482–491, 1964.
4. **Galer D, Leung H, Sussman R, Trzos R.** Scientific and practical considerations for the development of occupational exposure limits (OELs) for chemical substances. *Regul Toxicol Pharmacol* 15: 291–306, 1992.
5. **Grabarek Z, Gergely J.** Zero-length crosslinking procedure with the use of active esters. *Anal Biochem* 185: 131–135, 1990.
6. **Huang H, Kajiura H, Yamada A, Ata M.** Purification and alignment of arc-synthesis single-walled carbon nanotube bundles. *Chem Phys Lett* 356: 567–572, 2002.
7. **ICRP Task Group on Lung Dynamics.** Deposition and retention models for internal dosimetry of the human respiratory tract. *Health Phys* 12: 173–207, 1966.
8. **Junqueira LCU, Bignolas G, Brentani RR.** Picrosirius staining plus polarization microscopy, a specific method for collagen detection in tissue sections. *Histochem J* 11: 447–455, 1979.
9. **Kagan VE, Tyurina YY, Tyurin VA, Konduru NV, Potapovich AI, Osipov AN, Kisin ER, Schwegler-Berry D, Mercer RR, Shvedova AA.** Direct and indirect effects of single walled carbon nanotubes on RAW 264.7 macrophages: role of iron. *Toxicol Lett* 165: 88–100, 2006.
10. **Lam CW, James JT, McCluskey R, Hunter RL.** Pulmonary toxicity of single-wall carbon nanotubes in mice 7 and 90 days after intratracheal instillation. *Toxicol Sci* 77: 126–134, 2004.
11. **Langer KH, Thoenes W.** Characterization of cells involved in the formation of granuloma. *Virchows Arch B Cell Pathol Incl Mol Pathol* 36: 177–194, 1981.
12. **Malkusch W, Rehn B, Bruch J.** Advantages of sirius red staining for quantitative morphometric collagen measurements in lungs. *Exp Lung Res* 21: 61–77, 1995.
13. **Mangum J, Turpin E, Antao-Menezes A, Cesta M, Bermudez E, Bonner J.** Single-walled carbon nanotube (SWCNT)-induced interstitial fibrosis in the lungs of rats is associated with increased levels of PDGF mRNA and the formation of unique intercellular carbon structures that bridge alveolar macrophages in situ. *Part Fibre Toxicol* 3: 1–13, 2006.
14. **Maynard AD, Baron PA, Foley M, Shvedova AA, Kisin ER, Castranova V.** Exposure to carbon nanotube material: aerosol release during the handling of unrefined single-walled carbon nanotube material. *J Toxicol Environ Health* 967: 87–107, 2004.
15. **Mercer RR, Russell ML, Crapo JD.** Alveolar septal structure in different species. *J Appl Physiol* 77: 1060–1066, 1994.
16. **Mercer RR, Russell ML, Roggli VL, Crapo JD.** Cell number and distribution in human and rat airways. *Am J Respir Cell Mol Biol* 10: 613–624, 1994.
17. **Rao GVS, Tinkle S, Weissman DN, Antonini JM, Kashon ML, Salmen R, Battelli LA, Willard PA, Hubbs AF.** Efficacy of a technique for exposing the mouse lung to particles aspirated from the pharynx. *J Toxicol Environ Health* 66: 1441–1452, 2003.
18. **Sager T, Porter D, Robinson V, Lindsley G, Schwegler-Berry D, Castranova V.** Improved method to disperse nanoparticles for in vitro and in vivo investigation of toxicity. *Nanotoxicology* 2: 1–6, 2007.
19. **Shvedova AA, Kisin ER, Mercer R, Murray AR, Johnson VJ, Potapovich AI, Tyurina YY, Gorelik O, Arepalli S, Schwegler-Berry D, Hubbs AF, Antonini J, Evans DE, Ku BK, Ramsey D, Maynard A, Kagan VE, Castranova V, Baron P.** Unusual inflammatory and fibrogenic pulmonary responses to single-walled carbon nanotubes in mice. *Am J Physiol Lung Cell Mol Physiol* 289: L698–L708, 2005.
20. **Shvedova AA, Sager T, Murray AR, ERK, Porter D, Leonard S, Schwegler-Berry D, Robinson V, Castranova V.** Critical issues in the evaluation of possible effects resulting from airborne nanoparticles. In: *Nanotechnology: Characterization, Dosing and Health Effects*, edited by Monterro-Rivere NaVT. Philadelphia, PA: Informa Healthcare, 2007, p. 221–232.
21. **Sinnott S.** Chemical functionalization of carbon nanotubes. *J Nanosci Nanotech* 2: 113–123, 2002.

22. **Soler P, Bernaudin JF, Basset F.** Ultrastructure of pulmonary granulomatosis induced in rats by intravenous complete Freund's adjuvant. *Virchows Arch A Pathol Anat Histol* 368: 35–50, 1975.
23. **Stone KC, Mercer RR, Gehr P, Stockstill B, Crapo JD.** Allometric relationships of cell numbers and size in the mammalian lung. *Am J Respir Cell Mol Biol* 6: 235–243, 1992.
24. **Turk JL, Narayanan RB.** The monocyte-macrophage system in granulomatous inflammation. *Haematol Blood Transfus* 27: 101–107, 1981.
25. **Underwood EE.** *Quantitative Stereology.* Reading, MA: Addison-Wesley, 1970.
26. **Warheit D, Laurence B, Reed K, Roach D, Reynolds G, Webb T.** Comparative pulmonary toxicity assessment of single wall carbon nanotubes in rats. *Toxicol Sci* 26: 2281–2300, 2003.
27. **Xu X, Ray R, Gu Y, Ploehn H, Gearheart L, Raker K, Scrivens W.** Electrophoretic analysis and purification of fluorescent sing-walled carbon nanotube fragments. *J Am Chem Soc* 126: 12736–12737, 2004.
28. **Zeidler P, Hubbs AF, Battelli LA, Castranova V.** Role of nitric oxide synthase-derived nitric oxide in silica-induced pulmonary inflammation and fibrosis. *J Toxicol Environ Health* 67: 1001–1026, 2004.